Journal of Nano- and Electronic Physics
Vol. **17** No 6, 06032(10pp) (2025)

Журнал нано- та електронної фізики
Том **17** № 6, 06032(10cc) (2025)

OPEN ACCESS

REGULAR ARTICLE

Achieving 38.27 % Efficiency in CIGS Solar Cells Using V_2O_5 Back-Surface Field and Dual Window Layers: A Simulation Approach

Leila Naceri, Mousaab Belarbi*

Laboratory of Micro and Nanophysics – LaMiN, Department of FPST-École Nationale Polytechnique d'Oran-Maurice Audin, BP 1523, Oran 31000, Algeria

(Received 07 September 2025; revised manuscript received 14 December 2025; published online 19 December 2025)

This study explores the performance enhancement of Copper Indium Gallium Selenide (CIGS) solar cells using a novel AZO/SnO_2/ZnS/CIGS/V_2O_5/Ag heterostructure. Simulations with SCAPS-1D (Solar Cell Capacitance Simulator in One Dimension) software, compared three configurations: without a back-surface field (BSF) layer, with a $BaSi_2$ BSF layer, and with a V_2O_5 BSF layer. Incorporating the V_2O_5 BSF layer improved efficiency to 30.63 %. Optimization of key parameters, including absorber thickness (1 μm), defect density (10^{12} cm^{-3}), acceptor density (10^{19} cm^{-3}), electron affinity (4.2 eV), series resistance (0 Ω), and operating temperature (310 K), elevated performance, achieving an open-circuit voltage (V_{oc}) of 1.02 V, short-circuit current density (J_{sc}) of 43.01 mA/cm^2, fill factor (FF) of 86.68 %, and an efficiency (η) of 38.27 %. These improvements are attributed to the synergy between the dual window layers and the V_2O_5 BSF layer, which together reduced recombination losses and enhanced charge collection. The findings provide valuable insights into the design and development of cost-effective, high-performance, and sustainable CIGS solar cells, positioning this approach as a promising solution for advancing renewable energy technologies.

Keywords: CIGS solar cell, Back-surface field, Dual window layers, SCAPS-1D, Efficiency optimization.

DOI: 10.21272/jnep.17(6).06032 PACS numbers: 07.05.Tp, 88.40.jm

1. INTRODUCTION

The rapid growth of global population and industrialization has significantly increased greenhouse gas emissions and fossil fuel consumption, leading to critical issues such as global warming and resource depletion. To combat these challenges, the world urgently needs new, clean, and sustainable energy sources to replace fossil fuels. Among these alternatives, solar energy stands out as an abundant and renewable resource with immense potential [1].

Photovoltaic (PV) technology is central to harnessing solar energy, directly converting sunlight into electricity through the photovoltaic effect. This involves the absorption of photons by a semiconductor, creating electron-hole pairs that generate a potential difference when separated by a *p-n* junction, ultimately producing electric current [2]. To meet global energy demands, it is crucial to develop PV systems that are both cost-effective and efficient [3].

Among various PV technologies, copper indium gallium diselenide (CIGS)-based thin-film solar cells (TFSCs) have emerged as a promising solution due to their high conversion efficiency and excellent performance in outdoor conditions [4]. Although CIGS cells are more expensive to manufacture compared to other thin-film technologies like cadmium telluride (CdTe) or hydrogenated amorphous silicon (a-Si) [5], they offer superior efficiency. However, the scarcity and high cost of rare metals such as gallium (Ga) and indium (In) present significant challenges. Researchers are therefore focused on reducing the thickness of the CIGS absorber layer to decrease material costs while maintaining performance [6].

To further enhance the electrical characteristics and efficiency of CIGS cells, numerous studies have focused on improving traditional structures and proposing novel configurations. A significant approach involves the incorporation of an efficient back surface field (BSF), which has been shown to improve device efficiency and reduce absorber layer thickness. Since the 1980s, BSF layers have been recognized for their role in minimizing recombination rates, thereby increasing photocurrent and photovoltaic conversion efficiency [7-10].

Moreover, numerical simulations play a crucial role in advancing PV technology. Tools like SCAPS-1D are extensively used to study and optimize the optical and electrical properties of solar cells, providing valuable insights that drive the development of more efficient and cost-effective solar cells. These simulations help researchers fine-tune cell structures and parameters, leading to significant improvements in device performance [11].

Several studies exemplify the effectiveness of numerical simulations in improving solar cell efficiency. For instance, Ghobadi et al. conducted a computational analysis to explore the device characteristics of $Cu_2BaSnSSe_3$ (CBT(S,Se_3)) solar cells, utilizing SCAPS-1D simulations. To enhance cell performance and efficiency, they propose the incorporation of various Back Surface Field (BSF) layers on the absorber layer. Based on the optimal

* Correspondence e-mail: moussaab.belarbi@enp-oran.dz

Cite this article as: L. Naceri et al., *J. Nano- Electron. Phys.* 17 No 6, 06032 (2025) https://doi.org/10.21272/jnep.17(6).06032

parameters identified for an effective BSF layer, they simulated a $Cu_2BaSnSSe_3$ solar cell with SnS as the BSF layer, observing notable improvements in the cell's parameters. Notably, a peak power conversion efficiency (PCE) of 7.31 % was achieved [12].

Virang Shukla and Gopal Panda tackled CdTe's back surface ohmic contact issue with a novel Back Surface Field (BSF) material, boosting efficiency and stability. By incorporating Cu_2Te as the BSF layer and reducing CdS thickness to 5 nm, they achieved an impressive 19.06 % efficiency with just 1000 *nm* of CdTe, surpassing conventional cells' 14.87% efficiency with thicker layers [13].

Shamim Ahmmed et al. conducted a simulation study on CuO-based heterostructure solar cells using SCAPS-1D. By adjusting key parameters like CuO absorber thickness and the V_2O_5 back surface field (BSF) layer, they optimized performance. Their analysis also considered defect densities and optical losses, resulting in a solar cell with power conversion efficiency (PCE) of 12.09%. This study highlights the potential of CuO-based solar cells and the importance of simulation-driven optimization [14].

Ahmmed et al. investigated copper manganese tin sulfide (Cu_2MnSnS_4) for thin-film solar cells (TFSCs) using numerical simulations. They evaluated the performance of Cu_2MnSnS_4 (CMTS)-based TFSCs with and without a tin sulphide (SnS) back surface field (BSF) layer. Initially, they examined parameters like active material thickness, doping concentration, defect density, operating temperature, and metal contacts without a BSF layer. Subsequently, they optimized the cell by integrating SnS as a BSF layer in a heterostructure of Cu/ZnO/*i*-ZnO/*n*-CdS/*p*-Cu_2MnSnS_4/Pt. Their results showed a photoconversion efficiency (PCE) of 25.43 % without the SnS BSF layer, which increased to 31.4 % with the BSF layer. These findings highlight the potential of CMTS with SnS as both absorber and BSF layers for developing highly efficient solar cells [15].

Abdelmoumene Laidouci et al. conducted a numerical investigation into $ZnSnN_2$ solar cells using SCAPS-1D software. They analyzed how various parameters affect performance, including the thicknesses of the ZnO window layer, CdS buffer layer, $ZnSnN_2$ absorber layer, and Si back surface field (BSF) layer, as well as operating temperature, series and shunt resistances (R_S and R_{Sh}), defect density, and interface defects. A thin solar cell with a 1 μm thick absorber layer achieved an efficiency of 23.9 %. Optimizing conditions with an 8 μm absorber layer and a 0.3 μm BSF width, the cell showed resistances of $R_{Sh} = 10^6$ Ωcm^2 and $R_S = 1$ Ωcm^2, with a low defect density ($Nt = 10^{10}$ cm^{-3}), resulting in an efficiency of 29.5 %. The compound's abundance, non-toxicity, and cost-effectiveness make it appealing compared to conventional solar cells that use rare, toxic, and costly elements [16].

Md Islahur Rahman Ebon et al. explored a novel structure featuring antimony selenide (Sb_2Se_3), a promising absorber material for thin-film solar cells, coupled with a tungsten diselenide (WSe_2) back surface field (BSF). Using SCAPS-1D simulations, they investigated the properties that make Sb_2Se_3 suitable for non-toxic solar cell absorbers. Their study examined two structures: one with and one without a BSF layer. The results showed an efficiency of 20.61 % with an 800 nm thick absorber in the absence of a BSF layer. Adding a 100 nm WSe_2 BSF significantly increased efficiency to 32.35 %. These findings highlight the remarkable efficiency potential of this thin-film solar cell configuration [17].

Km. Kanchan et al. evaluated a thin-film solar cell (TFSC) featuring a copper-indium-gallium-diselenide (CIGS) absorber layer and a low-cost ultra-thin $BaSi_2$ back surface field (BSF) layer, structured as Al/SnO_2/buffer layer/CIGS/$BaSi_2$/Mo/substrate. Their objective was to enhance performance and reduce toxicity by replacing conventional CdS buffer layers with $Cd_{0.6}Zn_{0.4}S$ and ZnSe. They optimized the CIGS layer thickness (0.1 to 1 μm) for cost-effectiveness. The TFSC achieved maximum conversion efficiencies of 28.11 % with $Cd_{0.6}Zn_{0.4}S$ and 27.72 % with ZnSe for a CIGS thickness of 0.8 μm and a $BaSi_2$ BSF layer thickness of 0.3 μm. These results demonstrate performance improvements over previously reported CdS-based TFSCs [18].

Md. Ferdous Rahman and colleagues highlighted that solar cells utilizing copper indium gallium selenide (CIGS) show higher absorber efficiency compared to those using cadmium telluride (CdTe) or hydrogenated amorphous silicon (a-Si). They proposed a novel solar cell architecture incorporating CIGS within a multilayer structure of FTO, ZnSe, V_2O_5, and Cu. Using simulation tools, they evaluated various parameters, including the inclusion of a back-surface field (BSF) layer, absorber layer thickness, and acceptor density. Their results showed that a configuration with a 1 μm thick CIGS absorber, V_2O_5 BSF, and ZnSe layers achieved an efficiency of 31.86 % with a V_{OC} of approximately 0.9 V. This innovative design demonstrates significant potential for developing highly efficient solar cells, outperforming traditional designs [19].

In the same vein of research, Sayed Rezwanul Islam Biplab et al. affirmed that CIGS-based solar cells exhibit superior efficiency compared to other second-generation technologies like hydrogenated amorphous silicon (a-Si) or cadmium telluride (CdTe). However, they acknowledged the higher manufacturing cost associated with CIGS due to the use of rare metals like indium and gallium. To address this, they focused on enhancing efficiency with more economical materials. Their work introduced a back-surface field layer of low-cost barium silicide ($BaSi_2$) with a thickness of 0.3 μm into the basic CIGS solar cell structure. Using the simulation software SCAPS, they comprehensively studied all photovoltaic parameters. Their findings revealed that the proposed structure achieved an efficiency of 26.24 % with a thin CIGS layer of 0.8 μm. This novel approach not only reduced CIGS thickness and cost but also enhanced performance compared to conventional designs [20].

In our study, we aimed to enhance the performance of conventional CIGS solar cells by remodeling them with appropriate buffer and BSF layers between the absorber layer and the rear electrode. The buffer layer, positioned between the double window layers and the absorber, forms a *p*-*n* junction that helps eliminate defects and interfacial strain caused by the window layer. The BSF layer, with favorable physical, optical, and chemical stability, facilitates the effective transport and accumulation of photogenerated carriers from the absorber layer to the metal electrodes, significantly enhancing device efficiency and allowing for a reduced thickness of

the absorber layer. Furthermore, placing the BSF between the absorber and rear electrode can further reduce the absorber layer thickness, thereby lowering the overall cost of the PV cell. Using SCAPS-1D software, we designed and analyzed the structure of CIGS thin-film solar cells. First, we examined the *J-V* characteristics of our proposed structure, AZO/SnO_2/ZnS/CIGS/Ag, and introduced a BSF layer to enhance its efficiency. We compared two different BSF materials, $BaSi_2$ and V_2O_5, within this structure. Moreover, we optimized the device by investigating the effects of CIGS layer thickness, doping concentrations, electron affinity, and defect density on the *J-V* characteristics. We also explored the impact of series resistance and operating temperature on the solar cell's performance. Our optimized structure, featuring a double window layer of AZO/SnO_2 and a V_2O_5 BSF, achieved significantly improved photoconversion efficiency. These improvements highlight the potential for developing high-performance, cost-effective CIGS solar cells, paving the way for more sustainable and efficient photovoltaic technologies.

2. MATERIALS AND METHODS

2.1 Cell Structure

This study focused on simulating a solar cell. First, to calibrate the simulation setup, a CIGS-based solar cell reported in the literature [19, 20] was analyzed. Subsequently, three proposed structures were investigated, as shown in Figure 1. The first device structure, shown in Figure 1-A, does not include a BSF layer and consists of Al/AZO/SnO_2/ZnS/CIGS/Ag. The second and third device structures, shown in Figure 1-B and Figure 1-C respectively, incorporate BSF layers. The second structure comprises Al/AZO/SnO_2/ZnS/CIGS/ $BaSi_2$/Ag, while the third structure consists of Al/AZO/SnO_2/ZnS/CIGS/V_2O_5/Ag.

The proposed device structures use $BaSi_2$ and V_2O_5 as BSF layers, CIGS as a *p*-type absorber layer, ZnS as an *n*-type buffer layer, and a double window layer composed of (AZO+SnO_2). Silver (Ag) is used as the back contact, with a work function of 4.26 eV.

2.2 Numerical Modelling & Simulated Parameters

SCAPS-1D is a software tool developed by the Department of Electronics and Information Systems (EIS) at the University of Gent, Belgium, designed for simulating one-dimensional solar cells [11]. This program allows researchers to explore the impact of varying material properties, including the presence or absence of specific characteristics and their value ranges, on the efficiency of solar cells, thereby supporting optimization processes.

The parameters for our simulations were derived from both theoretical models and experimental data, as shown in Table 1. All simulations were conducted under standard conditions with a working temperature of 300 *K* and using the AM1.5 solar spectrum.

3. RESULTS AND DISCUSSIONS

3.1 *J-V* Characteristic of Proposed Structure

We simulated three different configurations of CIGS-based solar cells, with and without a BSF layer, as illustrated in Figure 1. The simulation results are summarized in Table 2 and the *J-V* curves are presented in Figure 2. The performance parameters include open-circuit voltage (*Voc*), short-circuit current density (*Jsc*), fill factor (*FF*), and efficiency (η).

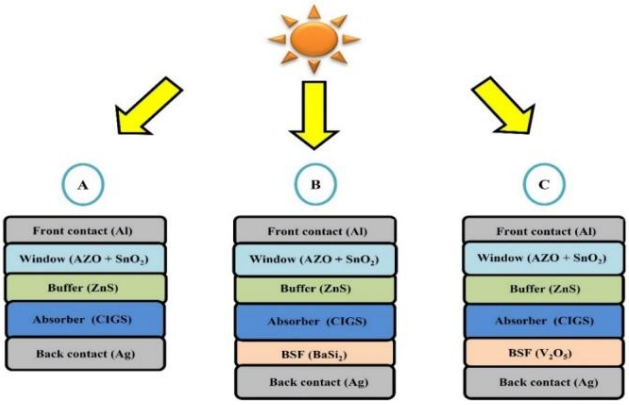

Fig. 1 – CIGS solar cell configurations: (A) No BSF layer, (B) $BaSi_2$ BSF layer, (C) V_2O_5 BSF layer

The results show that the addition of BSF layers significantly enhances the performance of the solar cells. The configuration without a BSF layer serves as the baseline. Introducing a $BaSi_2$ BSF layer significantly improves the *Voc*, *Jsc*, and efficiency. The configuration with a V_2O_5 BSF layer shows the best overall performance, achieving the highest values for *Voc*, *Jsc*, *FF*, and efficiency. The increase in *Voc* and *Jsc* with BSF layers indicates better carrier collection and reduced recombination losses, while the higher *FF* in the V_2O_5 configuration indicates more efficient charge separation and extraction. These results demonstrate that optimizing the BSF layers is crucial for enhancing the efficiency of CIGS thin-film solar cells.

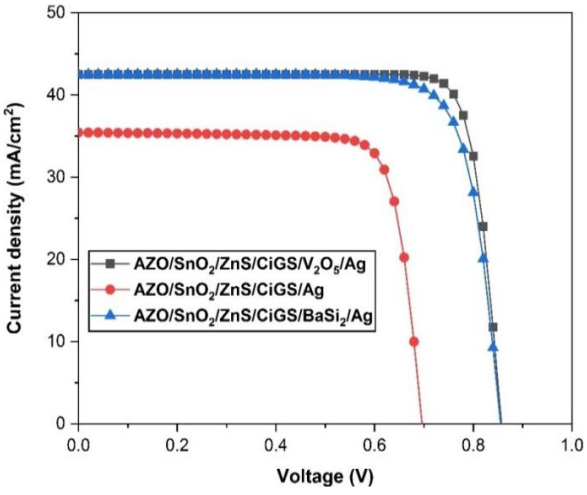

Fig. 2 – *J-V* characteristic with and without BSF layer

3.2 EQE & Energy Band for the Best Strucutre

The results indicate that introducing a BSF layer significantly enhances overall device performance. This improvement is attributed to the reduction in minority carrier recombination at the back surface of the device.

Table 1 – Material parameters used for simulation [14, 18-20]

Input parameters of the solar cell	Layers					
	AZO	**SnO_2**	**ZnS**	**CIGS**	**$BaSi_2$**	**V_2O_5**
Thickness (μm)	0.025	0.025	0.05	0.8	0.3	0.3
Band gap (eV)	3.4	3.6	2.4	1.1	1.3	2.2
Electron affinity (eV)	4.6	4.0	4.31	4.2	3.3	3.4
Permittivity (ε_r)	9	9	10	13.6	11.17	8
Nc (cm^{-3})	2.2×10^{18}	2.2×10^{18}	1.56×10^{18}	2.2×10^{18}	2.6×10^{19}	9.2×10^{19}
Nv (cm^{-3})	1.8×10^{19}	1.8×10^{19}	1.8×10^{19}	1.8×10^{19}	2×10^{19}	5.0×10^{20}
Hole mobility (cm^2/Vs)	25	25	25	25	100	100
Electron mobility (cm^2/Vs)	100	100	100	100	820	150
N_D (cm^{-3})	1.8×10^{20}	1×10^{18}	1×10^{17}	/	/	/
N_A (cm^{-3})	/	/	/	1×10^{18}	5×10^{18}	1×10^{19}
Defect (cm^{-3})	1×10^{15}	1×10^{15}	1×10^{15}	1.1×10^{14}	1×10^{15}	1×10^{14}

Table 2 – Output results of simulated structures.

Structures	Performance parameter			
	Voc **(V)**	***Jsc*** **(mA/cm^2)**	***FF*** **(%)**	***η*** **(%)**
AZO/SnO_2/ZnS/ CiGS/Ag	0.69	35.42	80.01	19.74
AZO/SnO_2/ZnS/ CiGS/$BaSi_2$/Ag	0.85	42.48	79.10	28.75
AZO/SnO_2/ZnS/ CiGS/V_2O_5/Ag	0.86	42.52	84.02	**30.63**

V_{OC}: Open-circuit voltage; J_{SC}: Short-circuit current density; *FF*: Fill factor; η: Efficiency

As shown in Figure 2, the solar cell with a V_2O_5 BSF layer demonstrates a substantial efficiency increase, confirming that our optimal structure is Al/AZO/SnO_2/ZnS/CIGS/V_2O_5/Ag. This indicates that the V_2O_5 layer effectively passivates the back surface and reduces carrier recombination losses, leading to improved carrier collection and higher device performance.

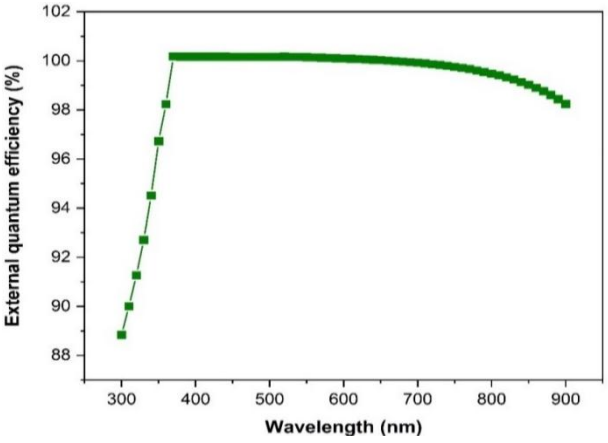

Fig. 3 – External quantum efficiency curve of the best structure

After confirming the best structure, we examined the external quantum efficiency (EQE) curve, also known as the spectral response curve, displayed in Figure 3. We observed an increased spectral response at shorter wavelengths, specifically between 300 nm and 400 nm. The high external quantum efficiency in this range suggests that the device is highly effective in generating electron-hole pairs from high-energy photons. The curve shows a peak efficiency of around 100 % within the wavelength range of 400 nm to 900 nm, indicating excellent photon absorption and charge collection in this range.

However, beyond 800 nm, the efficiency begins to decline, likely due to the incomplete absorption of longer-wavelength photons, which is a common limitation for CIGS-based solar cells due to their band gap.

The current passing through the heterojunction is determined by the band alignment. Figure 4 illustrates the energy band diagram for the proposed cell, based on the data obtained from the SCAPS simulation, showing the bandgap and layer thickness of each material. The diagram depicts the optimal structure, Al/AZO/SnO_2/ZnS/CIGS/V_2O_5/Ag.

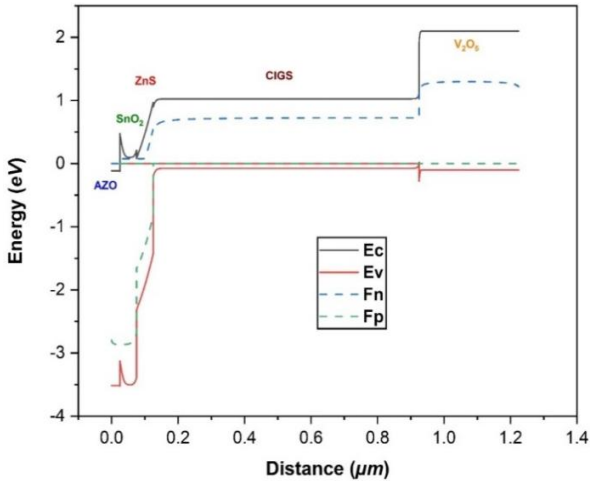

Fig. 4 – Energy band diagram of the best structure with the V_2O_5 BSF layer

In this configuration, Aluminum (Al) is used as the front grid contact, with a work function (WF) of 4.28 eV [21]. CIGS serves as the absorber layer, which is a *p*-type semiconductor with a bandgap of 1.1 eV [22]. ZnS is utilized as the *n*-type buffer layer with a bandgap of 2.4 eV [23, 24], while V_2O_5, with a bandgap of 2.2 eV, acts as the BSF layer to enhance the device's performance [25]. Additionally, AZO and SnO_2 are used as the double window layers, having bandgaps of 3.4 eV [26] and 3.6 eV [27], respectively. For the back contact layer, silver (Ag) is employed with a WF of 4.26 eV [28].

The energy band diagram in Figure 4 illustrates the favorable band alignment achieved with the materials used in the optimal structure, Al/AZO/SnO_2/ZnS/CIGS/

V_2O_5/Ag. The band bending at the V_2O_5 and CIGS junction creates an electric field that assists in the efficient separation and transport of photogenerated electron-hole pairs, reducing recombination and enhancing overall device performance. This alignment ensures that electrons and holes are effectively transported to their respective contacts, minimizing energy losses. The incorporation of V_2O_5 as a BSF layer optimizes the band structure and significantly contributes to the improved efficiency of the CIGS solar cells.

3.3 Influence of CIGS thickness

An absorber layer should be optimized to achieve the ideal thickness for maximum photon absorption and electron-hole pair generation. In this section, we examine the performance of the best structure: Al/AZO/SnO_2/ZnS/CIGS/V_2O_5/Ag, using the parameters listed in Table 1, to determine the best thickness for the CIGS absorber layer. Parameters such as open-circuit voltage (*Voc*), current density (*Jsc*), fill factor (*FF*), and efficiency (η) were assessed by varying the absorber layer thickness from 0.2 to 1.1 μm. The results, presented in Table 3, show that *Jsc*, *Voc*, and η increase with increasing absorber layer thickness up to a certain point.

Figure 5 illustrates the *J-V* curves for different thicknesses of the CIGS absorber layer. As the CIGS layer thickness is increased from 0.2 to 1.1 μm, *Jsc* significantly rises from 32.30 mA/cm² to approximately 43.14 mA/cm², and η rapidly increases from 24.31 % to about 30.77 %. *Voc* remains stable around 0.85 *V* and *FF* around 84 %. Beyond 1.1 μm, all photovoltaic properties remain nearly unchanged.

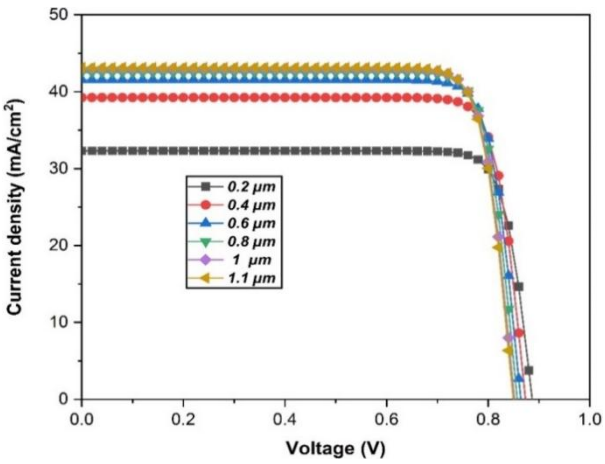

Fig. 5 – *J-V* curve of CIGS solar cells with various values of absorber layer thickness

This behavior results from enhanced photon absorption and increased electron-hole generation in the CIGS absorber layer. Therefore, a thickness of 1.0 μm is determined to be the optimal thickness for the CIGS absorber layer in an efficient Al/AZO/SnO_2/ZnS/CIGS/V_2O_5/Ag solar cell [29]. This optimization ensures that the solar cell can achieve maximum efficiency without unnecessary material usage, balancing performance with cost-effectiveness.

Table 3 – Performance results due to variation in thickness of absorber layer

Thickness (μm) CIGS	Performance Parameter			
	Voc (V)	*Jsc* (mA/cm²)	*FF* (%)	η (%)
0.2	0.88	32.30	84.88	24.31
0.4	0.87	39.24	84.42	28.94
0.6	0.86	41.55	84.16	30.22
0.8	0.85	42.52	84.02	30.63
1	0.85	42.99	84.01	**30.77**
1.1	0.85	43.14	83.97	30.76

Voc: Open-circuit voltage; *Jsc*: Short-circuit current density; *FF*: Fill factor; η: Efficiency.

3.4 CIGS Defect and Acceptor Density

To investigate the impact of defect density in the CIGS layer on the photovoltaic performance of the solar cell, we varied the single-donor-type bulk defect density from 1×10^{11} to 1×10^{16} cm^{-3} while keeping the defect densities of all other layers constant, as specified in Table 1. Figure 6 illustrates how different defect densities affect the efficiency of the solar cell. The conversion efficiency decreases from 35 % at a defect density of 1×10^{12} cm^{-3} to 24 % at a defect density of 1×10^{16} cm^{-3}.

As defect density increases, the probability of carrier recombination rises before the carriers can contribute to current generation [30]. This means a higher defect density results in fewer electron-hole pairs contributing to the current, leading to lower efficiency.

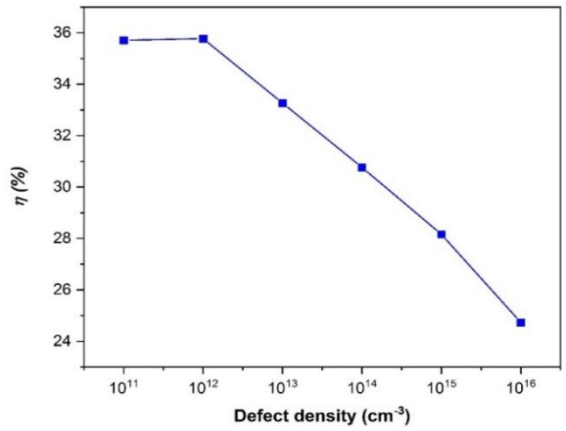

Fig. 6 – Effect of defect density variations in the CIGS layer on solar cell efficiency

Previous studies [31, 32], have shown that defects significantly deteriorate photovoltaic performance by acting as recombination centers for charge carriers, thus reducing the efficiency of the solar cell. To enhance the output of the proposed cell, it is crucial to minimize the defect density in the absorber layer, ideally keeping it below 1×10^{13} cm^{-3}. Our results indicate that the optimal absorber defect density is 1×10^{12} cm^{-3}, resulting in an efficiency of 35.77 %.

Defects in the CIGS material affect its electronic properties by increasing the recombination rate of electrons and holes [33], altering the band gap, and reducing the mobility of charge carriers. These effects can lead to

a decrease in the performance of CIGS solar cells by limiting the effective generation and collection of charge carriers.

The acceptor concentration in the CIGS layer also plays a significant role in determining the performance of CIGS-based solar cells. We varied the acceptor concentration N_A in the absorber layer from 10^{12} to 10^{20} cm^{-3}, and the simulated photovoltaic efficiencies are displayed in Figure 7. The figure shows that the efficiency increases significantly as N_A rises from 10^{12} to 10^{20} cm^{-3}, with an optimal efficiency of 38.23 % achieved at an acceptor concentration of about 10^{19} cm^{-3}. Beyond this value, the efficiency decreases sharply [34].

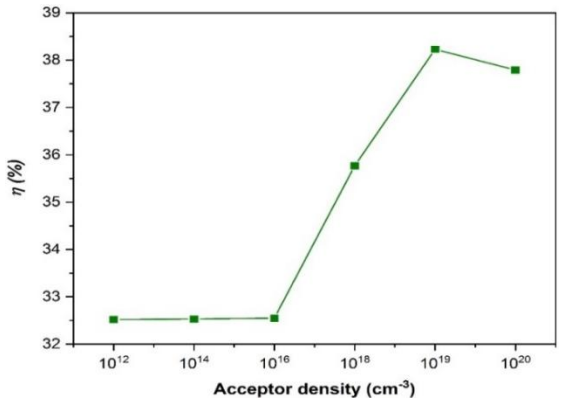

Fig. 7 – Effect of varying acceptor density in the CIGS layer on solar cell efficiency

An increase in the acceptor density enhances the electric field within the absorber layer, improving charge separation and reducing recombination. However, excessively high acceptor densities can lead to a decrease in mobility due to increased scattering, resulting in lower efficiency [31, 35]. Our findings suggest that for optimal performance, the acceptor concentration in the CIGS layer should be higher than 10^{16} cm^{-3} and lower than 10^{19} cm^{-3}.

3.5 CIGS Electron Affinity

At the interface between the absorber and buffer layers in a solar cell, electron affinity plays a crucial role in defining the conduction band offset. This offset significantly affects the open-circuit voltage, short-circuit current, and overall performance of the solar cell. Various research papers on CIGS solar cells have reported different values for electron affinity, including 4.45 eV [36], 4.2 eV [37], and 4.58 eV [38].

As illustrated in Figure 8, an increase in electron affinity leads to a decrease in efficiency for the CIGS absorber layer. This is because higher electron affinity reduces the conduction band offset at the interface, which can create a barrier to electron transport from the buffer to the absorber layer. This barrier can impede the collection of photo-generated electrons, reducing the current produced and thereby lowering the short-circuit current and overall efficiency of the solar cell.

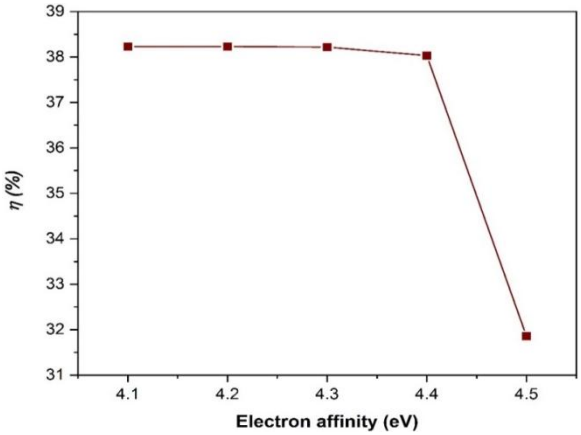

Fig.8 – Effect of electron affinity on the efficiency of CIGS absorber layer

For optimal performance, the electron affinity of the CIGS layer has been set to 4.2 eV, achieving an efficiency of 38.23 %. At this electron affinity, the conduction band offset is minimized, facilitating efficient electron transport across the interface. However, if the electron affinity is too high, it increases the barrier height, making it harder to collect photo-generated charge carriers and thus reducing the overall performance of the device.

This highlights the importance of carefully tuning the electron affinity to balance efficient carrier collection with minimal recombination losses.

3.6 Influence of Resistance Serie

In this study, the effect of series resistance (R_s) on the photovoltaic device is investigated using SCAPS-1D software. Series resistance arises from the front and back metallic contact resistance, bulk resistance, and circuit terminal resistance. The primary impact of series resistance is to reduce the fill factor (*FF*), making it impossible to achieve an *FF* of 100 %. To enhance efficiency, it is essential to minimize series resistance. This resistance also affects the open-circuit voltage (V_{OC}) and short-circuit current (J_{SC}). Lower *Rs* is desirable for improving the power conversion efficiency (η).

The value of R_s is varied from 0 (*ideal case*) to 6 Ω. Figure 9 illustrates the effect of changing R_s on the optimal cell configuration, which includes the V_2O_5 BSF layer. The figure shows that increasing R_s significantly degrades the efficiency of the solar cell. As R_s increases, the efficiency of the solar cell decreases markedly, dropping from 38.23 % to 27.97 %. Similarly, as shown in Table 4, both *FF* and efficiency decrease continuously with increasing R_s, while *Voc* and *Jsc* remain almost constant. The nearly constant *Voc* and *Jsc* values indicate that series resistance primarily affects the internal resistance of the cell, not the carrier generation and separation processes. As R_s increases, the fill factor and efficiency decrease significantly due to higher power losses [38]. Minimizing series resistance is therefore essential in the design and fabrication of solar cells to maintain high efficiency and performance.

Table 4 – Performance results of variation in series resistance for the proposed structure

R_s (Ω)	Performance Parameter			
	Voc (V)	*Jsc* (mA/cm²)	*FF* (%)	*η* (%)
0	1.03	43.01	86.11	**38.23**
1	1.03	43.01	82.22	36.50
2	1.03	43.01	78.33	34.77
3	1.03	43.01	74.45	33.05
4	1.03	43.01	70.56	31.32
5	1.03	43.01	66.67	29.59
6	1.03	43.01	63.00	27.97

Voc: Open-circuit voltage; *Jsc*: Short-circuit current density; *FF*: Fill factor; *η*: Efficiency.

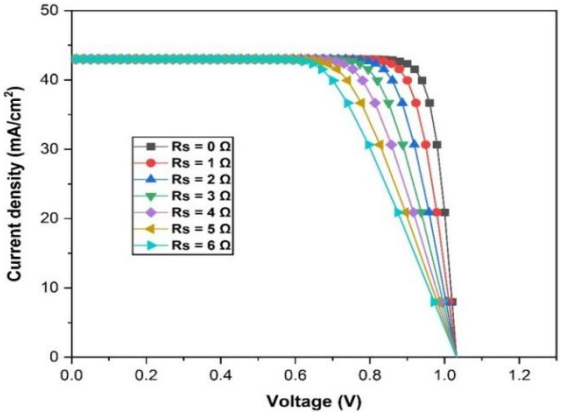

Fig. 9 – Impact of varying series resistance on the proposed structure

3.7 Influence of Temperature

The operating temperature of a solar cell is a crucial factor that affects its performance and stability. Excessive heat can damage photovoltaic (PV) cells and shorten their lifespan, making temperature control essential for outdoor installations. This section examines the influence of temperature on the performance of the optimal solar cell configuration. By maintaining constant parameters and varying the operating temperature from 280 to 330 K, we analyzed the photovoltaic performance of the cells. As shown in Table 5 and Figure 10, temperature variations have a significant impact on key performance metrics such as open-circuit voltage, short-circuit current, fill factor, and efficiency. Lower temperatures generally enhance cell performance, while higher temperatures degrade it.

Table 5 – Performance Results for Varying Operating Temperatures of the Proposed Structure.

T (K)	Performance Parameter			
	Voc (V)	*Jsc* (mA/cm²)	*FF* (%)	*η* (%)
280	1.04	43.01	84.15	37.72
290	1.03	43.01	85.14	37.98
300	1.03	43.01	86.11	38.23
310	1.02	43.01	86.68	**38.27**
320	1.02	43.01	86.86	38.14
330	1.01	43.01	86.75	37.88

The results indicate that the efficiency of the solar cell improves as the temperature decreases from 330 K to 280 K. The highest efficiency of 38.27% is achieved at 310 K. This improvement at lower temperatures is attributed to reduced recombination rates, which increase carrier lifetimes and enhance overall efficiency. Conversely, higher temperatures increase thermal energy, leading to higher recombination rates and reduced carrier mobility, negatively impacting efficiency [39]. These findings emphasize the importance of thermal management in the design and deployment of photovoltaic systems to ensure stable and high performance.

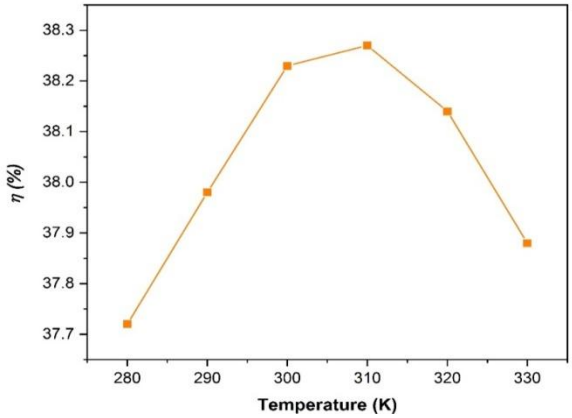

Fig.10 – Effect of operating temperature on the efficiency of the optimal solar cell structure

3.8 Optimized vs. Initial Structure

In the final phase of our investigation, we aimed to present the optimal configuration for our proposed structure after thorough research. This optimized configuration achieves maximum efficiency and performance through careful selection of appropriate device parameters. Initially, we simulated the structure Al/AZO/SnO_2/ZnS/CIGS/V_2O_5/Ag, achieving a conversion efficiency of 30.63 %.

We then optimized the CIGS absorber layer to a thickness of 1 μm, set the defect density to 10^{12} cm^{-3}, and the acceptor density to 10^{19} cm^{-3}. We also determined the optimal electron affinity to be 4.2 eV. Furthermore, we found that the series resistance should be R_s = 0 Ω and the optimal operating temperature to be 310 K. The calculated parameters for the optimized and initial cells are presented in Table 6, which shows a significant improvement in cell efficiency from 30.63 % to 38.27 %. The current-voltage characteristic curves of the optimal CIGS solar cell, presented in Figure 11, demonstrate enhanced efficiency compared to the initial structure. The optimized structure shows improvements in all key performance metrics, underscoring the importance of the optimization process. These improvements highlight the potential for achieving high-efficiency solar cells through careful optimization of material and device parameters.

3.9 Comparison with Previous Studies

Our investigation has led to the identification of an optimal structure that significantly enhances the efficiency and overall performance of CIGS solar cells.

Various materials such as SnS, Si, $BaSi_2$, and others have been studied as the BSF layer for CIGS-based solar cells. Table 7 provides a comparative analysis of the photovoltaic performance between our optimized configuration and other studies on CIGS cells [19-20, 40], displaying the favorable impact of using a V_2O_5 BSF in CIGS-based solar cells.

Table 6 – Comparison of simulation results: optimized vs. initial structure

Stuctures	V_{OC} (V)	J_{SC} (mA/cm²)	*FF* (%)	η (%)
Initial	0.86	42.52	84.02	30.63
Optimized	1.02	43.01	86.68	38.27

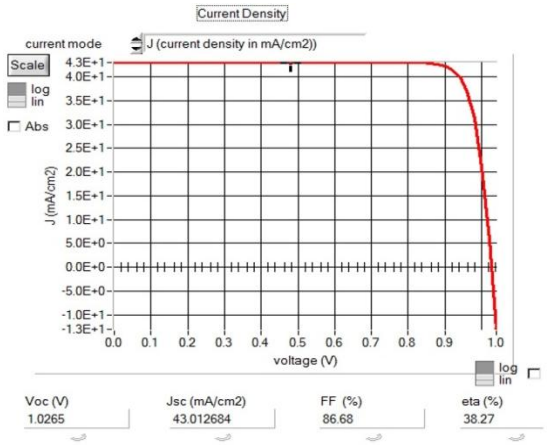

Fig.11– *J-V* characteristic of the optimized structure

The results indicate that the V_2O_5 BSF demonstrates superior performance compared to other BSF layers. The higher bandgap of 2.2 eV for the V_2O_5 BSF layer allows the device to operate efficiently at higher temperatures, thus enhancing its overall performance compared to other BSF materials. This high bandgap helps in better carrier separation and reduces recombination losses, which are critical for improving the efficiency of solar cells.

Our optimized structure, which includes a 1 μm thick CIGS absorber layer, not only achieves high efficiency but also offers commercial feasibility. The reduction in the thickness of the absorber layer lowers the material costs, making the production of these solar cells more cost-effective. This study demonstrates that with the appropriate optimization of device parameters, CIGS solar cells can achieve high performance, making them a promising candidate for widespread commercial use.

4. CONCLUSIONS

In this study, we conducted a comprehensive numerical simulation to examine the electrical properties of CIGS-based solar cells using the SCAPS-1D software. Our investigation focused on the integration of a double window layer and a back surface field (BSF) layer to enhance device performance. We designed three different configurations: a baseline without a BSF layer, a second with a $BaSi_2$ BSF layer, and a third with a V_2O_5 BSF layer. The configuration with the V_2O_5 BSF layer emerged as the most efficient, achieving a significant improvement in efficiency to 30.63 %. Further optimization involved adjusting critical parameters for the CIGS absorber layer, including its thickness (1 μm), acceptor density (10^{19} cm^{-3}), defect density (10^{12} cm^{-3}), and electron affinity (4.2 eV). The optimized cell configuration, incorporating a V_2O_5 BSF and ZnS buffer with AZO and SnO_2 double window layers, demonstrated substantial enhancements in current density, voltage, and overall efficiency, while also reducing the required thickness of the absorber layer. We also assessed the influence of series resistance and operating temperature on the solar cell's performance.

The optimal performance was achieved with a series resistance of R_s = 0 Ω and an operating temperature of 310 K, resulting in a peak efficiency of 38.27 %. Our findings provide essential insights and guidelines for designing high-performance, cost-effective, and environmentally sustainable CIGS-based thin-film solar cells.

The successful implementation of a thin CIGS absorber layer with a V_2O_5 BSF layer underscores the potential for these optimized structures in practical solar energy applications. Future research should focus on exploring the long-term stability and environmental durability of V_2O_5 BSF layers in CIGS solar cells, as well as their integration into other types of photovoltaic technologies.

AKNOWLEDGEMENTS

We extend our sincere thanks to Professor Marc Burgelman and his team at Ghent University, Belgium, for providing access to the SCAPS simulation software.

Table 7 – Performance Comparison of Photovoltaic Structures with Different BSF Layers.

Structures	References	V_{OC} (V)	J_{SC} (mA/cm²)	*FF* (%)	η (%)
Al/SnO_2:F/$Cd_{0.6}Zn_{0.4}S$/CIGS/$BaSi_2$/Mo	[18]	0.90	41.21	75.76	28.11
FTO/ZnSe/CIGS/V_2O_5/Cu	[19]	0.89	41.34	85.80	31.86
Al/FTO/CdS/CIGS/$BaSi_2$/Mo	[20]	0.84	40.56	76.80	26.24
Al/ITO/Al-ZnO/*i*-ZnO/CIGS/PbS/Mo	[40]	0.83	35.22	82.29	24.22
AZO/SnO_2/ZnS/CIGS/V_2O_5/Ag	**[This work]**	1.02	43.01	86.68	**38.27**

REFERENCES

1. Shahab Eslami, Aslan Gholami, Amin Bakhtiari, Majid Zandi, Younes Noorollahi, *Energy Convers. Manag.* **200**, 112107 (2019).
2. J.JM. Halls, C.A. Walsh, N.C. Greenham, E.A. Marseglia, R.H. Friend, S.C. Moratti, AB Holme, *Lett. Nat.* **50**, 13 (1995).
3. Salh Alhammadi, Hyeonwook Park, Woo Kyoung Kim, *Materials* **12** No 9, 1365 (2019).
4. Amal Bouich, Bouchaib Hartiti, Shafi Ullah, Hanif Ullah, Mohamed Ebn Touhami, D.M.F. Santos, Bernabé Marí Soucase, *Optik* **183**, 137 (2019).
5. Md. Mahabub Alam Moon, Md. Ferdous Rahman, Jaker Hossain, Abu Bakar Md. Ismail, *Adv. Mater. Res.* **1154**, 102 (2019).
   Chiara Candelise, Jamie F. Speirs, Robert J.K. Gross, *Renew. Sustain. Energy Rev.* **15** No 9, 4972 (2011).
6. J.C.C. Fan, M.B. Spitzer, R.P. Gale, *High-Efficiency III–V Solar Cells. Advances in Solar Energy*, **6** (Ed. by K.W. Böer) (Springer, Boston, MA: 1990).
7. P.D. DeMoulin, M.S. Lundstrom, R.J. Schwartz, *Sol. Cell.: Sci., Technol., Appl. Econ.* **20**, 229 (1987).
8. Sabrina Benabbas, Zahir Rouabah, Nadir Bouarissa, Nacereddine Chelali, *Optik Int. J. Light Electron Opt.* **127** No 15, 6210 (2016).
9. Sangho Kim, Vinh Ai Dao, Chonghoon Shin, Nagarajan Balaji, Junsin Yi, *J. Nanosci. Nanotechnol.* **14** No 12, 9258 (2014).
10. J. Verschraegen, M. Burgelman, *Thin Solid Films* **515**, 6276 (2007).
11. A. Ghobadi, M. Yousefi, M. Minbashi, A.H. Ahmadkhan Kordbacheh, A.R. Haji Abdolvaha, N.E. Gorjii, *Opt. Mater.* **107**, 109927 (2020).
12. Virang Shukla, Gopal Panda, *Mater. Today: Proc.* **44**, 2300 (2021).
13. Shamim Ahmmed, Asma Aktar, Samia Tabassum, Md. Hafijur Rahman, Md. Ferdous Rahman, Abu Bakar Md. Ismail, *Superlattice. Microst.* **151**, 106830 (2021).
14. Ahmmad Isha, Abu Kowsar, Abdul Kuddus, M. Khalid Hossain, Md Hasan Ali, Md Dulal Haque, Md Ferdous Rahman, *Heliyon* **9**, e15716 (2023).
15. Abdelmoumene Laidouci, Mamta, V.N. Singh, Pratap Kumar Dakua, Deepak Kumar Panda, *Heliyon* 9, e20601 (2023).
16. Md Islahur Rahman Ebon, Md Hasan Ali, Md Dulal Haque, Abu Zafor Md Touhidul Islam, *Eng. Res. Express* **5**, 045072 (2023).
17. Km Kanchan, Sahu Anupam, Yadav Shivangi, *J. Nano-Electron. Phys.* **15** No 2, 02025 (2023).
18. Md. Ferdous Rahman, Nayeem Mahmud, Intekhab Alam, Md Hasan Ali, Md. Mahabub Alam Moon, Abdul Kuddus, G. F. Ishraque Toki, Mirza Humaun Kabir Rubel, Abdullah Al Asad, and M. Khalid Hossain, *AIP Adv.* **13** No 04, 045309 (2023).
19. Sayed Rezwanul Islam Biplab, Md Hasan Ali, Md. Mahabub Alam Moon, M. Firoz Pervez, Md. Ferdous Rahman, Jaker Hossain, *J. Comput. Electron.* **19**, 342 (2019).
20. Rakib Hosen, Sawrab Sikder, Md. Shihab Uddin, Md. Manjurul Haque, Hayati Mamur, Mohammad Ruhul Amin Bhuiyan, *J. Alloy. Metallurg. Syst.* **4**, 100041 (2023).
21. M. Topić, F. Smole, J. Furlan, *Sol. Energy Mater. Sol. C.* **49**, 311 (1997).
22. Samer H. Zyoud, Ahed H. Zyoud, Naser M. Ahmed, Atef F. I. Abdelkader, *Crystals* **11**, 1454 (2021).
23. Md Noumil Tousif, Sakib Mohammad, A.A. Ferdous, Md Ashraful Hoque, *J. Clean Energy Technol.* **6**, 293 (2018).
24. M. Khalid Hossain, A.A. Arnab, Ranjit C. Das, K.M. Hossain, MH. K. Rubel, Md. Ferdous Rahman, H. Bencherif, M.E. Emetere, Mustafa K.A. Mohammed, Rahul Pandey, *RSC Adv.* **12**, 34850 (2022).
25. Izzeddine Belkacem, Souhila Bensmaine, Mousaab Belarbi, Chams El Hayat Merzouk, *Semicond. Sci. Technol* **39**, 115005 (2024).
26. M. Belarbi, O. Zeggai, S. Louhibi-Fasla, *Mater. Today: Proc.* **51** Part 7, 2115 (2022).
27. A. Benyoucef, M. Belarbi, O. Zeggai, S. Goumri-Said, M.B. Kanoun, B. Benyoucef, S. Louhibi-Fasla, *Physica Scripta* **98** No 9, 095009 (2023).
28. Mohamed Wahid Bouabdelli, Fatiha Rogti, Mostefa Maache, Abdelaziz Rabehi, *Optik* **216**, 164948 (2020).
29. Deli Li, Lin Song, Yonghua Chen, Wei Huang, *Adv. Sci.* **7**, 1901397 (2020).
30. Hocine Heriche, Zahir Rouabah, Nadir Bouarissa, *Int. J. Hydrogen Energy* **42** No 15, 9524 (2017).
31. Sabrina Benabbas, Zahir Rouabah, Hocine Heriche, Nacer-Eddine Chelali, *Afr. J. Sci. Technol. Innov. Dev.* **8** No 4, 340 (2016).
32. Ranbir Singh, Sanjay Sandhu, Jae-Joon Lee, *Sol. Energy* **193**, 956 (2019).
33. M. Belarbi, O. Zeggai, S. Louhibi-Fasla, *J. Renew. Energ.* **1** No 01, 31 (2022).
34. Adama Sylla, Siaka Touré, Jean-Pierre Vilcot, *Open J. Model. Simul.* **5** No 4, 218 (2017).
35. Djimba Niane, Ibrahima Wade, Ousmane Diagne, Mouhamadou M.Socé, Moustapha Dieng, *Am. J. Energy Res.* **6**, 42 (2018).
36. Samaneh Sharbati, Sayyed Hossein Keshmiri, J. Tyler McGoffin, Russell Geisthardt, *Appl. Phys. A* **118**, 1259 (2014).
37. L. Naceri, M. Belarbi, *Physica Scripta* **99** No 3, 035028 (2024).
38. Mousaab Belarbi, Oussama Zeggai, Sami Khettaf, Souad Louhibi-Fasla, *Semicond. Sci. Technol.* **9** No 37, 095016 (2022).
39. B. Barman, P.K. Kalita, *Sol. Energy* **216**, 329 (2021).

Досягнення ефективності 38,27% у сонячних елементах CIGS з використанням поля V_2O_5 на задній поверхні та шарів подвійного вікна: підхід моделювання

Leila Naceri, Mousaab Belarbi

Laboratory of Micro and Nanophysics – LaMiN, Department of FPST-École Nationale Polytechnique d'Oran-Maurice Audin, BP 1523, Oran 31000, Algeria

У роботі проведено дослідження підвищення продуктивності сонячних елементів на основі селеніду міді та індію-галію (CIGS) з використанням нової гетероструктури AZO/SnO_2/ZnS/CIGS/V_2O_5/Ag. Моделювання за допомогою програмного забезпечення SCAPS-1D (Solar Cell Capacitance Simulator in One Dimension) порівнювало три конфігурації: без шару заднього поля (ШЗП), з шаром ШЗП $BaSi_2$ та з шаром ШЗП V_2O_5. Включення шару ШЗП V_2O_5 підвищило ефективність до 30,63 %. Оптимізація ключових параметрів, включаючи товщину поглинача (1 мкм), густину дефектів (10^{12} $см^{-3}$), густину акцептора (10^{19} $см^{-3}$), спорідненість до електрона (4,2 еВ), послідовний опір (0 Ом) та робочу температуру (310 К), підвищила продуктивність, досягнувши напруги холостого ходу (V_{oc}) 1,02 В, густини струму короткого замикання (J_{sc}) 43,01 мА/$см^2$, коефіцієнта заповнення (FF) 86,68 % та ефективності (Ω) 38,27 %. Ці покращення пояснюються синергією між шарами подвійного вікна та шаром V_2O_5 ШЗП, що разом зменшило втрати на рекомбінацію та покращило збирання заряду. Отримані результати дають цінну інформацію про проектування та розробку економічно ефективних, високопродуктивних та екологічно чистих сонячних елементів CIGS, позиціонуючи цей підхід як перспективне рішення для розвитку технологій відновлюваної енергетики.

Ключові слова: Сонячний елемент CIGS, Поле на задній поверхні, Подвійні віконні шари, SCAPS-1D, Оптимізація ефективності.